J Comput Aided Mol Des (2009) 23:501–511
DOI 10.1007/s10822-009-9288-x

Fragment-based lead generation: identification of seed fragments by a highly efficient fragment screening technology

Lars Neumann · Allegra Ritscher · Gerhard Müller · Doris Hafenbradl

Received: 4 May 2009 / Accepted: 20 May 2009 / Published online: 17 June 2009

Abstract For the detection of the precise and unambiguous binding of fragments to a specific binding site on the target protein, we have developed a novel reporter displacement binding assay technology. The application of this technology for the fragment screening as well as the fragment evolution process with a specific modelling based design strategy is demonstrated for inhibitors of the protein kinase p38alpha. In a fragment screening approach seed fragments were identified which were then used to build compounds from the deep-pocket towards the hinge binding area of the protein kinase p38alpha based on a modelling approach. BIRB796 was used as a blueprint for the alignment of the fragments. The fragment evolution of these deep-pocket binding fragments towards the fully optimized inhibitor BIRB796 included the modulation of the residence time as well as the affinity. The goal of our study was to evaluate the robustness and efficiency of our novel fragment screening technology at high fragment concentrations, compare the screening data with biochemical activity data and to demonstrate the evolution of the hit fragments with fast kinetics, into slow kinetic inhibitors in an in silico approach.

Keywords Fragment screening · Kinetic screening · Fragment evolution · Reporter displacement · Residence time · Deep-pocket binding · Retro-design

L. Neumann · A. Ritscher · D. Hafenbradl (✉)
Proteros Biostructures GmbH, Am Klopferspitz 19,
82152 Martinsried, Germany
e-mail: hafenbradl@proteros.com

G. Müller
Proteros Fragments GmbH, Fraunhoferstr. 20,
82152 Martinsried, Germany

Introduction

Fragment-based lead generation has matured over the last decade into a widely applied approach within pre-clinical research [1]. Within that concept, the combinatorial scenario in traditionally pursued lead finding, i.e., the systematic variation of several substituents mounted onto an underlying scaffold, is decomposed to few individual optimization tasks of less overall complexity. Thus, screening fragment libraries of hundreds or only a few thousand compounds generally yields in higher hit rates [2]. It has been shown that fragment libraries allow for a better sampling of the chemical space [3], and, given the cross-target promiscuity of less complex compounds [4], also the biological target space is explored more efficiently by fragments. In addition, novel binding modes of chemical substructures emerge that go undetected if those substructures are embedded in lead-like structures of increased complexity [5].

A key success factor for fragment based lead finding, as for any targeted drug discovery approach, is the rapid establishment of a structural and functional context, on which strategic decisions for subsequent optimization campaigns can be based. For fragment selection and fragment evolution rapid structure determination by e.g., protein crystallography is mandatory in order to gain insight into the primary interacting functionalities of the seed fragment, but also to fully rationalize the complete pharmacophoric requirements of the binding site which will govern the subsequent growth process of a seed fragment towards a more evolved lead compound. Apart from steric and physicochemical complementarity to the target protein's binding site, numerous additional parameters have to be improved, such as solubility, permeability, stability, etc. Only recently, the concept of efficient binding kinetics

emerged as a key optimization parameters in lead finding and optimization, generally aiming at inhibitors, agonists, or antagonists that exhibit a prolonged binary complex residence time, i.e., the period for which the target is occupied by the low-molecular weight ligand [6–8]. In numerous cases it has been shown that a prolonged residence time correlates with increased cellular, and ultimately in vivo efficacy. Apart from that pharmacodynamic aspect, the concept of residence time also has major implications on pharmacokinetic attributes. Whenever an extended effect of the drug over time is required in vivo, a long residence time helps to overcome the pharmacokinetic shortcomings of an inhibitor. Progression of a compound to in vivo studies not only requires a binding kinetic characterisation of the inhibitor against it's main target, but also to understand the kinetic selectivity of such a compound that is a direct correlate to off-target mediated toxicity [6–8].

A prolonged interaction time is typically based either on e.g., covalent binding of the compound, or on conformational changes of the target protein. For protein kinases, proteases and other target families it has been shown that small molecule inhibitors, agonists, or antagonists with a long residence time are superior compounds in the in vivo setting (see for example [9]).

The lack of high throughput technologies for measuring the residence time throughout a lead finding and optimization program has limited the number of programs where the residence time has actually been used in parallel to affinity data, thus rendering the entire concept as widely underappreciated in the medicinal chemistry community.

To improve the likelihood of finding compounds which show an increased residence time on the target, high throughput screening can be used employing specifically developed technologies which allow the identification of such molecular entities from chemical libraries, thus providing more interesting starting points for following optimization programs when compared to compounds that do not exhibit any kinetic signature.

Within our protein kinase programs, we have established the retro-design strategy where we set out to identify fragments that are specifically designed to bind to the deep pocket of kinases in their DFG-out conformation (Fig. 1).

This approach has a number of advantages when compared to traditional, hinge-directed kinase inhibitor approaches, since no prior optimization of typical heterocyclic core structures in terms of hydrogen bonding potential and patentability is required [10, 11]. In addition, the spatial evolution of a deep-pocket accommodated seed fragment towards the adenine binding site yields in kinase inhibitors of dramatically reduced molecular complexity, thereby avoiding a variety of traditionally encountered liabilities in e.g., the ADME profile. As a proof-of-concept

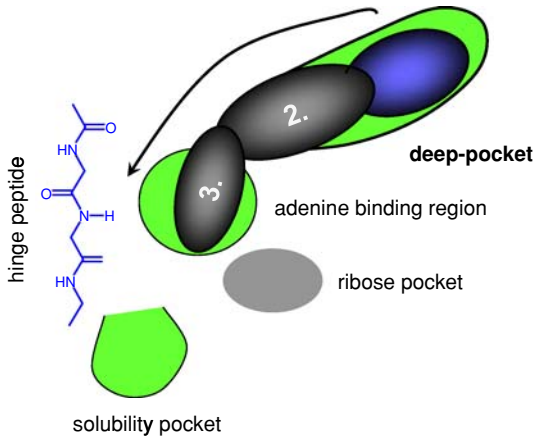

Fig. 1 Schematic representation of the "retro-design" approach embedded in a prototypic kinase inhibitor binding site. The seed fragment (*1*) is accommodated by the deep pocket, thus stabilizing the DFG-out conformation. Subsequently, seed fragment (*1*) is expanded over a back-pocket binding linker (*2*) to a hinge-binding entity (*3*)

study, we have chosen the protein kinase p38alpha for which we have established our in-house assay technology and conducted a fragment screen. This target enzyme is one of the most intensively studied systems in terms of binding kinetics of efficient kinase inhibitors with BIRB796 being one of the first compounds for which the DFG-out conformation of protein kinases has been experimentally determined [12, 13] We considered this system as the ideal showcase to demonstrate the efficiency and viability of our in-house developed approach towards fragment-based lead discovery for novel kinase inhibitors.

The goal of this study was to evaluate the robustness and efficiency of our novel fragment screening technology, to compare the screening data with biochemical activity data and to devise a strategy how to evolve the fragment hits showing fast kinetics, into slow kinetic inhibitors employing an in silico approach based on protein modelling technologies [14].

Materials and methods

Reporter displacement assay

The Proteros reporter displacement assay is based on a reporter probe that is distinctively designed to bind to the site of interest of the chosen target enzyme or receptor. The proximity between reporter and protein results in the emission of an optical signal. Fragments that bind to the same binding site are displacing the probe and causing signal loss (Fig. 2). The Proteros reporter displacement assay is a homogeneous method that can be used for all types of enzymes and receptors. A special prerequisite of the enzyme or receptor is not required. Due to the nature of

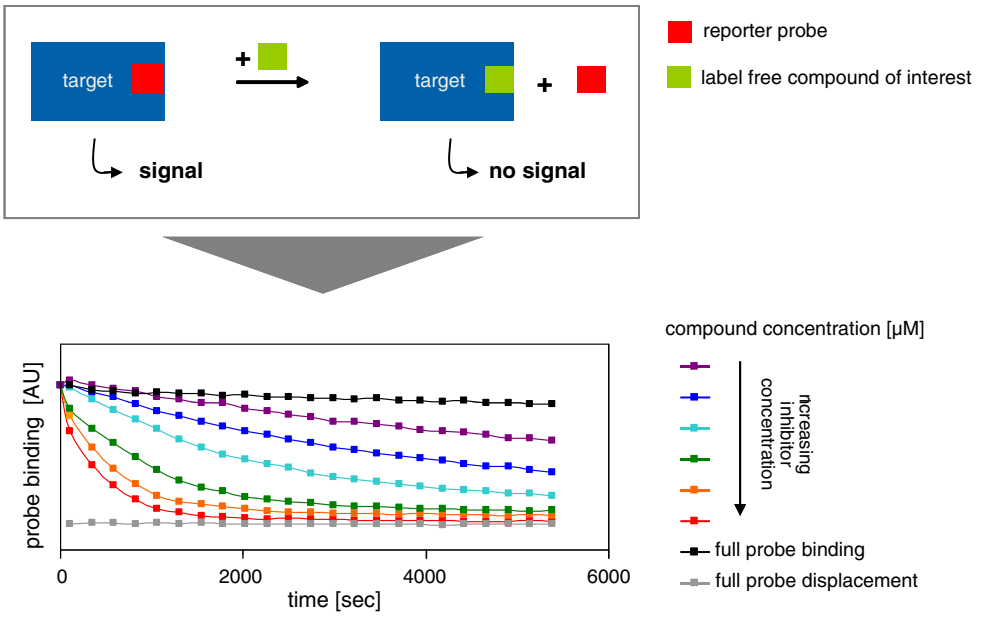

Fig. 2 Assay principle of reporter displacement assay. Binding of the reporter probe generates a specific signal. Displacement of the reporter probe by a competing compound of interest results in signal loss. By analyzing the kinetics of signal loss at various compound concentrations values as K_d, k_{on}, k_{off} and residence time can be calculated

the optical signal interference by the optical properties of compounds or fragments is very limited.

The reporter displacement assay was performed in a volume of 8 µL per well within a 384 well low volume plate. About 2 nM activated p38α was mixed with a 29 nM ATP site specific reporter probe in 20 mM Mops pH 7.0, 1 mM DTT, 0.01% Tween20. After 60 min incubation fragments were added at the desired concentration. Displacement of the reporter probe was measured either after 60 min incubation or continuously over time. The signal for full probe binding was measured in the absence of compound and the signal for complete reporter displacement was quantified in the absence of p38α.

Enzymatic p38α assay

Enzymatic p38α assays were performed using the IMAP technology (MDS analytic Technologies). The desired fragment concentration was mixed wit 50 nM activated p38α, 400 nM fluorescein labelled substrate peptide IPTTPITTTYFFFK-5Fl-COOH and 1.7 µM ATP in 8 µL 20 mM Mes pH 6.5, 0.4 mM $MgCl_2$, 0.4 mM $MnCl_2$, 1 mM DTT, 0.01% NP40. After 60 min incubation reaction was stopped by adding IMAP binding solution and p38α activity was quantified my measuring fluorescence polarization.

Molecular modelling

The most interesting fragments identified from screening of our in-house library were structurally evaluated in the context of their binding potential towards the deep-pocket of the p38alpha target kinase. For that purpose, we used manual docking and energy refinement based on molecular mechanics simulations. The high-resolution x-ray structure of p38alpha in complex with a DFG-out binding inhibitor (PDB code: 1WBS) was used, since this structure was of high-resolution (1.8 Å) and contained a well-resolved activation loop [15]. For efficient molecular mechanics studies, the pdb file was subjected to a refined simulation protocol using the consistent valence force field as embedded in the Discover simulation package [16], in order to remove any strain from the protein complex. Only a single kinase monomer has been extracted from the coordinate set. After protonation, the crystallographically derived protein complex was subjected to a sequence of energy minimization simulations. Initially, the system was minimized without any partial charges for 2,500 steps using the conjugate gradients algorithm with a tethering applied to all heavy atoms (force constant: 100 kJ mol^{-1}). In order to prevent any unwanted surface contraction phenomena, the binary protein complex was soaked by adding ~6,000 distinct water molecules to a sphere around the complex with a thickness of 15 Å. The soaked complex was further minimized over 5,000 steps conjugate gradient minimization with a position restraining applied to the heavy atoms of the protein and the ligand (force constant: 100 kJ mol^{-1}), thus allowing to water shell to adapt to the protein surface. Over further 5,000 steps of energy minimization the tethering was gradually removed and a final run of 2,500 steps of minimization was performed without any restraints on the system. After removing the inhibitor, the resulting protein structure was

then used to dock and refine the fragments within the inhibitor binding site.

Fragments were manually docked to the deep pocket in different poses, thus providing distinct starting configurations for energy minimization and molecular dynamics simulations. As mentioned above, all simulations were carried out after adding a 15 Å layer of water molecules around the respective fragment-kinase complexes. Each starting structure was subjected to a 5,000 step energy minimization protocol with an elaborated tethering strategy in order to smoothly remove any manually created gradients on the energy surface. After energy minimization, 50 ps of molecular dynamics simulations at an elevated temperature of 500 K were used to investigate the stability of the different docking poses. It should be emphasized that our intention was not to study the details of the protein dynamics, we wanted to explore the configurational and conformational plausibility of the initially made assumptions referring binding site and binding mode of the different inhibitor fragments.

Results and discussion

Fragment binding screen against p38α

About 1,023 fragments of the Proteros fragment library were screened in triplicates against the activated form of p38α using the Proteros reporter displacement assay. p38α was incubated with a reporter probe that was specifically designed to bind to the ATP binding site of p38α. Thereafter 2 mM of an individual fragment was added per well of a 384 well screening plate and probe displacement was measured (Fig. 2). On each screening plate the signal corresponding to 100% (absence of p38α) and 0% (absence of competing fragment) reporter displacement was measured in six wells, respectively. Assay stability was controlled by plotting signals for 100% and 0% reporter displacement for each screening plates (Fig. 3a). In addition assay significance was controlled by calculating the *z* prime for each screening plate (Fig. 3b). The *z* prime values for all screening plates were above 0.68 demonstrating the high significance of the screen. The *z* prime value for total screen considering all screening plates was calculated to be 0.72.

Fragments that bind to the ATP binding site of p38α were indentified by quantifying reporter probe displacement and the hit rate was calculated grouped by degree of reporter displacement (Table 1).

Inspection of the structures of all fragments with more than 50% probe displacement resulted in a list of 21 fragments for further characterization. For these fragments the IC50 values were measured using the Proteros reporter displacement assay and in addition an enzymatic p38α assay (Table 2). In order to measure also the IC50 value of fragments with very low affinities a fragment concentration of up to 22.61 mM was used. For the reporter displacement assay the reporter probe concentration was adjusted to its own K_d value and for the enzymatic assay the ATP concentration was adjusted to the Km_{app}(ATP) of p38α. Thus, according to the Cheng Prusoff equation [17] in both assays the resulting IC50 values equal two times the K_d value and are directly comparable.

From the 21 hit fragments from the primary screening effort, 17 fragments could be verified as p38α binders by measuring a valid IC50 curve with the reporter displacement assay resulting in a verification rate of 81%.

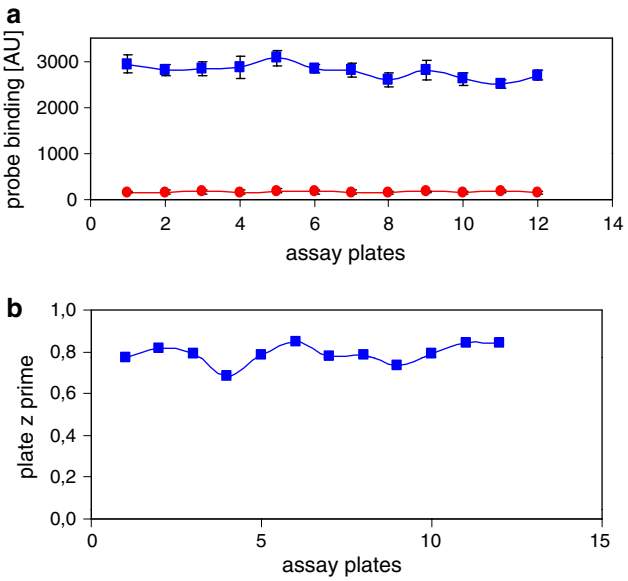

Fig. 3 Assay stability and assay significance was controlled by monitoring **a** the signals corresponding to 100% probe binding (absence of competing fragment) (*squares*) and 0% probe binding (absence of p38α) (*circles*) and **b** by calculating the *z* prime value for each screening plate. *Error bars* correspond to the standard deviation out of six wells

Table 1 Hit rate of 1023 fragments screened for their ability to compete with an ATP site specific reporter probe

Reporter displacement (%)	# Fragments	Hit rate (%)
>90	2	0.2
>80	8	0.8
>70	16	1.6
>60	32	3.1
>50	69	6.7

The signal corresponding to 100% reporter displacement was measured in the absence of p38α, while the signal for 0% reporter displacement was quantified in the absence of a competing fragment

Table 2 Comparison of the reporter displacement data resulting from the screen of the 1,023 fragments with the IC50 values generated with the reporter displacement binding assay and the enzymatic p38α assay

Fragment	Screen, reporter displacement (%)	IC50 (μM), reporter displacement assay	IC50 (μM), enzymatic assay
PRS-000553	81	248	890
PRS-001009	65	280	>22,610
PRS-000223	67	318	>22,610
PRS-001007	72	353	>22,610
PRS-000460	66	541	>22,610
PRS-000859	70	596	989
PRS-000793	57	703	14,594
PRS-000286	83	786	>22,610
PRS-000751	63	928	>22,610
PRS-000058	50	1,056	3,546
PRS-000419	53	1,213	>22,610
PRS-000787	54	1,360	10,021
PRS-000832	58	1,379	2,116
PRS-000145	55	1,701	4,368
PRS-000844	53	1,729	4,504
PRS-000789	56	1,945	>22,610
PRS-000807	50	5,490	>22,610
PRS-000164	57	>22,610	>22,610
PRS-000107	53	>22,610	>22,610
PRS-000117	53	>22,610	>22610
PRS-000978	75	>22,610	11,647

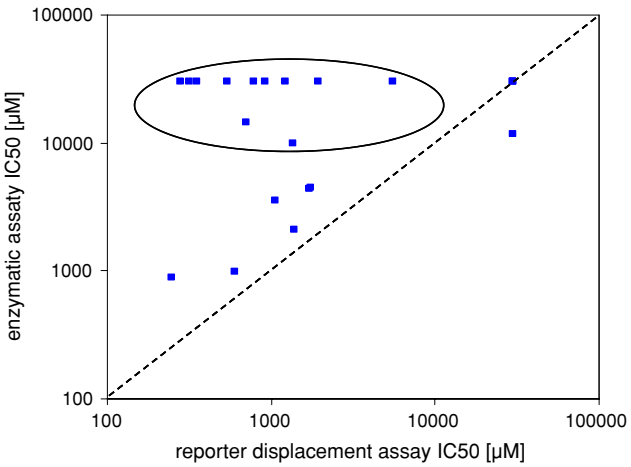

Fig. 4 IC50 values generated by the reporter displacement and the enzymatic p38α assay were plotted. Fragments with an IC50 values higher as the highest fragment concentration used for the IC50 determination (=22,610 μM) were plotted as 30,000 μM. Group I fragments, that show binding activity in the reporter displacement assay but no or only minor activity in the enzymatic assay are *circled*. Group II fragments that show binding activity and activity in the enzymatic assay are aligning along the *dashed identity line*

Interestingly not all of the p38α binding fragments showed activity in the enzymatic assay (Fig. 4). The p38α binding fragments can be divided into two groups: Group I fragments demonstrate binding activity by displacing the reporter probe but show no activity in the enzymatic assay and group II fragments that show similar IC50 values in the reporter displacement and the enzymatic assay. From the 17 verified hits from the initial screen 11 belong to group I. About 9 from these 11 fragments did not show any activity and 2 fragments only very weak activity in the enzymatic assay. The remaining 6 fragments are group II fragments and show good correlation between binding and enzymatic IC50 values. Although the authors cannot provide a full explanation for this observation we follow the hypotheses that group II fragments and ATP share the same binding regions within the ATP binding site of p38α. In consequence the fragments are ATP competitive and block enzymatic activity of p38α. In contrast group I fragments bind in regions of the ATP binding pocket that is utilized by the reporter probe only but not by ATP, as e.g., the back pocket. Thus both ATP and the fragment can bind to p38α at the same time while reporter probe and fragment cannot. In consequence group I fragments are able to displace the reporter probe but not ATP.

Kinetic characterization of p38α binding fragments

The binding kinetics of 3 fragments (PRS-000419, PRS-000223 and PRS-000058) that showed a particular structural similarity to the p38α inhibitor BIRB 796 were analyzed in detail. In addition the binding kinetics of BIRB 796 and two BIRB 796 fragments which have been described in literature [12, 13, 18] (Fig. 5) were measured in parallel. The same reporter probe that was used for the fragment screen was loaded to the ATP binding site of p38α. Thereafter fragments were added at increasing concentrations and reporter probe displacement was monitored continuously over time (Fig. 5). The reporter probes are designed to have fast association and dissociation kinetics in order to ensure that fragment binding and not reporter probe dissociation is the rate limiting step. Thus the signal decay describes directly the p38α association of the fragment. For technical reason the first measurement could be taken 40 s after fragment addition. For the fragments PRS-000419, PRS-000223, PRS-000058 and for the smaller fragment of the published BIRB 796 fragments binding equilibrium was reached already within these 40 s. The sensograms for all four compounds showed no concentration dependent variation over time (Fig. 5). Thus binding kinetics for these four compounds are faster than the detection limit of the reporter displacement assay (Table 3).

However, for the larger BIRB 796 fragments and for BIRB 796 itself the binding kinetics could be clearly

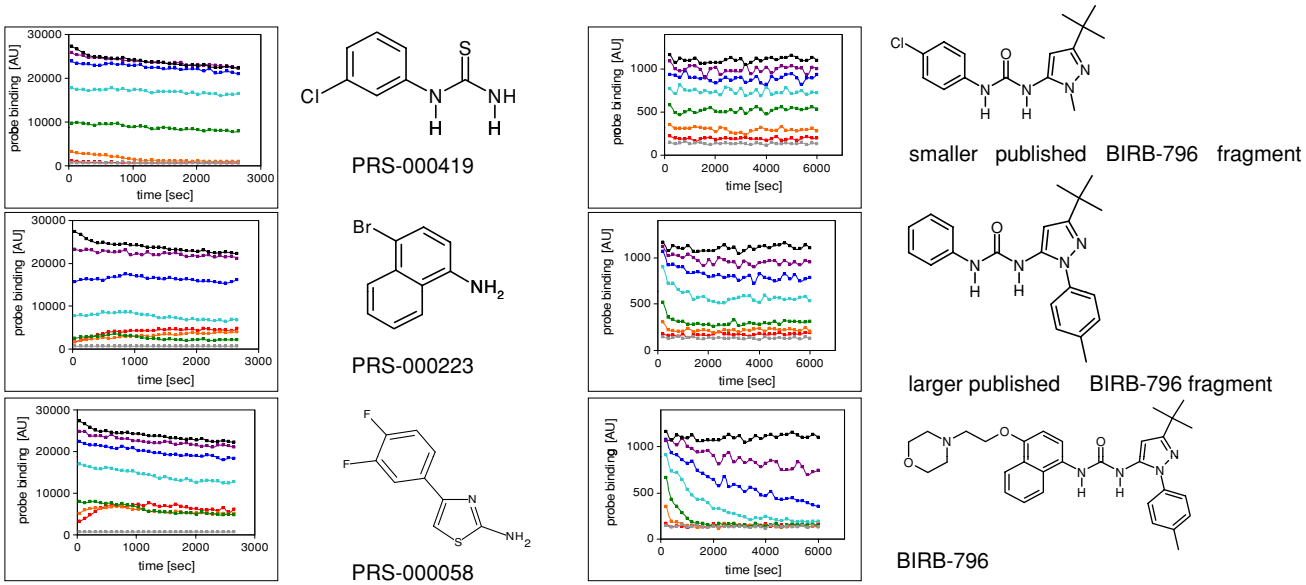

Fig. 5 Binding kinetics of fragments PRS-000419, PRS-000223, PRS-000058, two published BIRB 796 fragments and BIRB 796 itself were monitored using the reporter displacement assay. The reporter probe with fast p38α association and dissociation kinetics was bound the ATP binding site of p38α and fragments were added at six increasing concentrations (2.5, 0.9, 0.3, 0.1, 0.03, 0.01 μM for the smaller and larger published fragments of BIRB-796 and BIRB-796 and 20,000, 6,700, 2,200, 750, 250, 83 μM for PRS-000419, PRS-000223, PRS-000058 are marked in *red*, *orange*, *green*, *light blue*, *dark blue*, *purple*, respectively). Reporter displacement was observed continuously over time. In order to ensure appropriate mixing the first measurement was taken 40 s after fragment addition. 100% reporter displacement was measured in the absence of p38α (*grey*), while the signal for 0% reporter displacement was monitored in the absence of competing fragment (*black*)

Table 3 Binding kinetics between fragments/inhibitors and p38α as determined by reporter probe displacement assay

Inhibitor/fragment	K_d (μM)[a]	k_{on} (1/M 1/s)	k_{off}, 10^{-4} × (1/s)	Residence time (min)
PRS-00058	528	>100,000	>50	Below detection limit
PRS-000223	159	>100,000	>50	Below detection limit
PRS-000419	607	>100,000	>50	Below detection limit
Smaller BIRB-796 fragments	800	>100,000	>50	Below detection limit
Larger BIRB-796 fragments	32	19,400	9	18.5
BIRB-796	7	9,911	1.3	128

[a] Measured with reporter probe displacement assay. Reporter probe concentration was adjusted to K_d(probe). Thus K_d = ½ IC50 [17]

measured and time dependency of the binding events is clearly visible in the sensograms (Fig. 5).

In order to calculate k_{on} and k_{off} of the p38α—inhibitor interaction signal the observed association rate k_{obs} was determined for each inhibitor concentration by fitting the corresponding signal decay by fitting with a mono exponential decay equation (Fig. 6). The exponential coefficient of each mono exponential fit equals k_{obs} for the particular inhibitor concentration. The resulting k_{obs} values were plotted against their inhibitor concentration and fitted to Eq. (1) describing the dependency between the observed association rate k_{obs}, the association rate k_{on}, the dissociation rate k_{off} and the inhibitor concentration. The dissociation rate k_{off} is given by the *y*-intercept and the association rate k_{on} by the slope of dependency between k_{obs} and [inhibitor] (Fig. 6). Residence time was calculated by Eq. (2) [6].

$$k_{obs} = k_{off} + k_{on}\,[\text{inhibitor}] \quad (1)$$

$$\text{Residence time} = 1/k_{off} \quad (2)$$

Molecular modelling of selected fragments

To provide a structural understanding on the putative interaction modes of some of the identified fragments in the context of the target kinase binding site, docking followed by molecular mechanics simulations have been applied. To study potential binding modes, we decided to focus on three distinct fragments, notably the thio-urea PRS-000419, the aminothiazole PRS-000058, and the thiophene-containing carboxamide PRS-001007, the latter being a

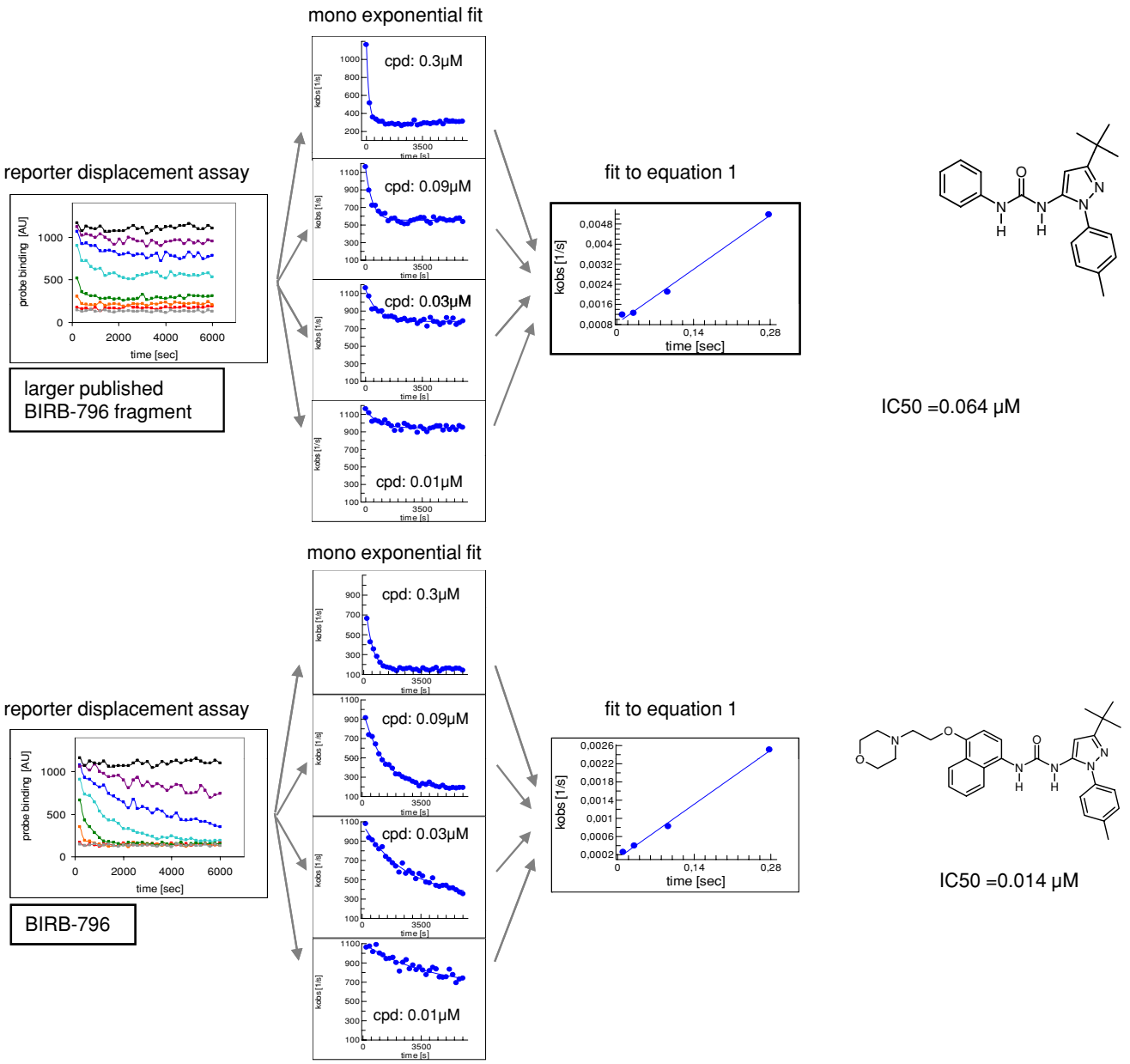

Fig. 6 The exponential coefficient k_{obs} for each inhibitor concentration was calculated by fitting the signal decays with a mono exponential decay equation. The k_{obs} values were plotted against the corresponding inhibitor concentration and k_{on} and k_{off} was determined by fitting to Eq. (1). For the plot only k_{obs} values were used that were well defined. Those k_{obs} values were omitted from analysis if signal decay for a particular inhibitor concentration was faster than the detection limit of the reporter displacement assay or if at low inhibitor concentration no significant reporter displacement occurred

fragment uncovered by the binding assay, but not showing enzymatic activity within the sensitivity range of the activity assay (Fig. 7). As outlined above, PRS-001007 can be considered as competitively displacing the applied probe compound, but not directly interfering with ATP. Intentionally, we also decided not to include the naphthaline derivative PRS-000223, since the compound exhibits only minor correspondence to any useful anchor point within the deep pocket of the target enzyme's binding site.

Under the assumption that deep pocket binding occurs for all three ligands, different starting positions were generated by superimposing the thio-urea, the aminothiazole, and the carboxamide onto the urea moiety of BIRB796 in its bound state (mutual superposition of 1WBS and 1KV2). For the aminothiazole, also known to be a prominent hinge binding group, we only focussed on deep pocket binding. For each fragment two distinct starting configurations were generated, given the pseudo-

symmetry around the urea, or urea-mimicking moiety in each studied fragment (Fig. 7).

The solvent shell consisting of ~6,000 distinct water molecules efficiently prevented the protein complexes from e.g., vacuum-derived contractions (Fig. 8).

Analysis of the molecular dynamics trajectories reveals that the protein oscillates around an average conformation without any remarkable conformational rearrangements or distortions of the backbone, thus rendering the chosen relaxation and simulation approach a viable procedure to reach equilibrium conditions (Fig. 9).

From detailed analyzes of the different simulations it turns out that the size of the explored conformational and

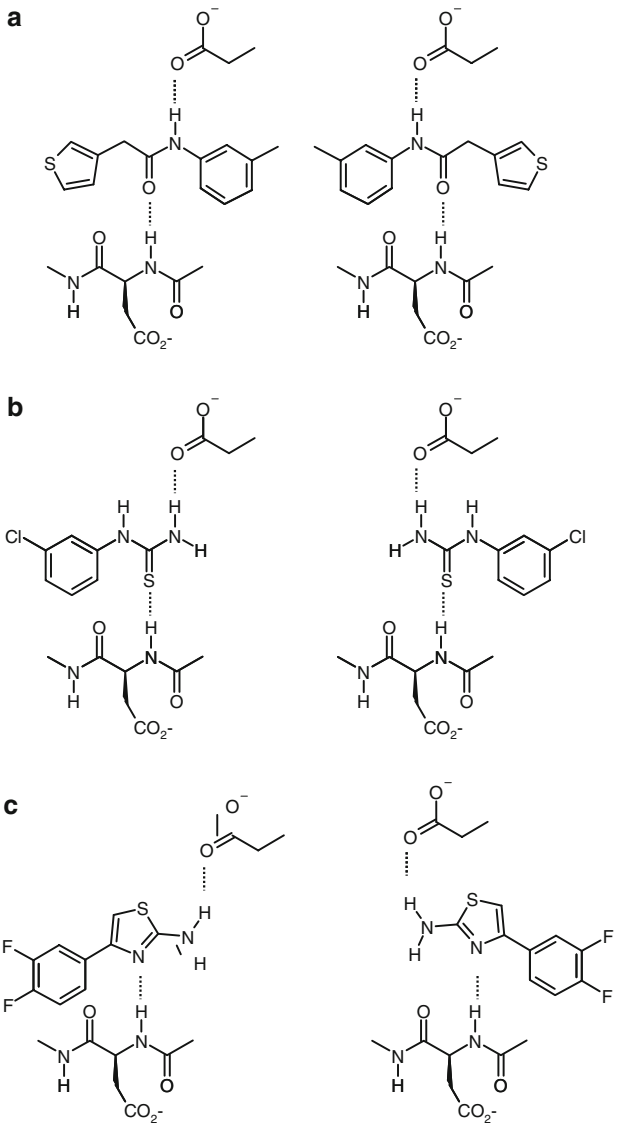

Fig. 7 Chemical structures of three fragment hits (**a** PRS-001007, **b** PRS-000419, **c** PRS-000058) that have been scrutinized by docking and energy refinement. For each compound, the two distinct docking poses are depicted schematically

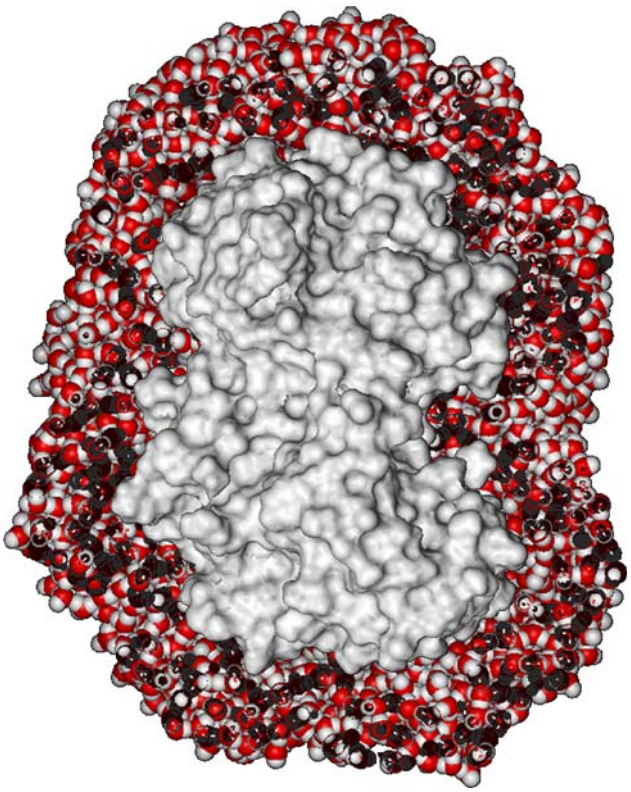

Fig. 8 Cross-section through the solvent shell around a kinase-fragment complex: Water molecules are shown as CPK models, the protein is surrounded by a solid Connolly surface

configurational space very much depends on the modelled ligand and the chosen binding mode (Fig. 7).

Despite the fact that all ligands were anchored with their functional groups (amide, thio-urea, aminothiazole) between the backbone NH of Asp-168 (hydrogen bond donor to the fragments) and the sidechain carboxylate of Glu-71 (accepts hydrogen bond from the fragments), various different degrees of conservation of these stabilizing interactions have been detected (Fig. 10).

The most conserved and restricted conformational and configurational performance was obtained for PRS-001007 with an initial binding mode in which the thiophene is oriented towards the interior of the binding pocket, resembling the vectorial direction towards the adenine binding area close to the hinge region (Fig. 10, upper panel, right). For the reverse binding mode, increased mobility of the fragment has been detected during the MD simulation (Fig. 10, upper panel, left). For the thio-urea fragment PRS-000419 a reasonable binding mode was analyzed in which the chloro-phenyl ring is accommodated by the hydrophobic pocket connecting the deep-pocket with the hinge region (Fig. 10, middle panel, left). In most of the snapshots of the MD simulation, interactions between the thio-urea and the Glu-71 and Asp-168 are found. Starting from the reversed binding mode with the

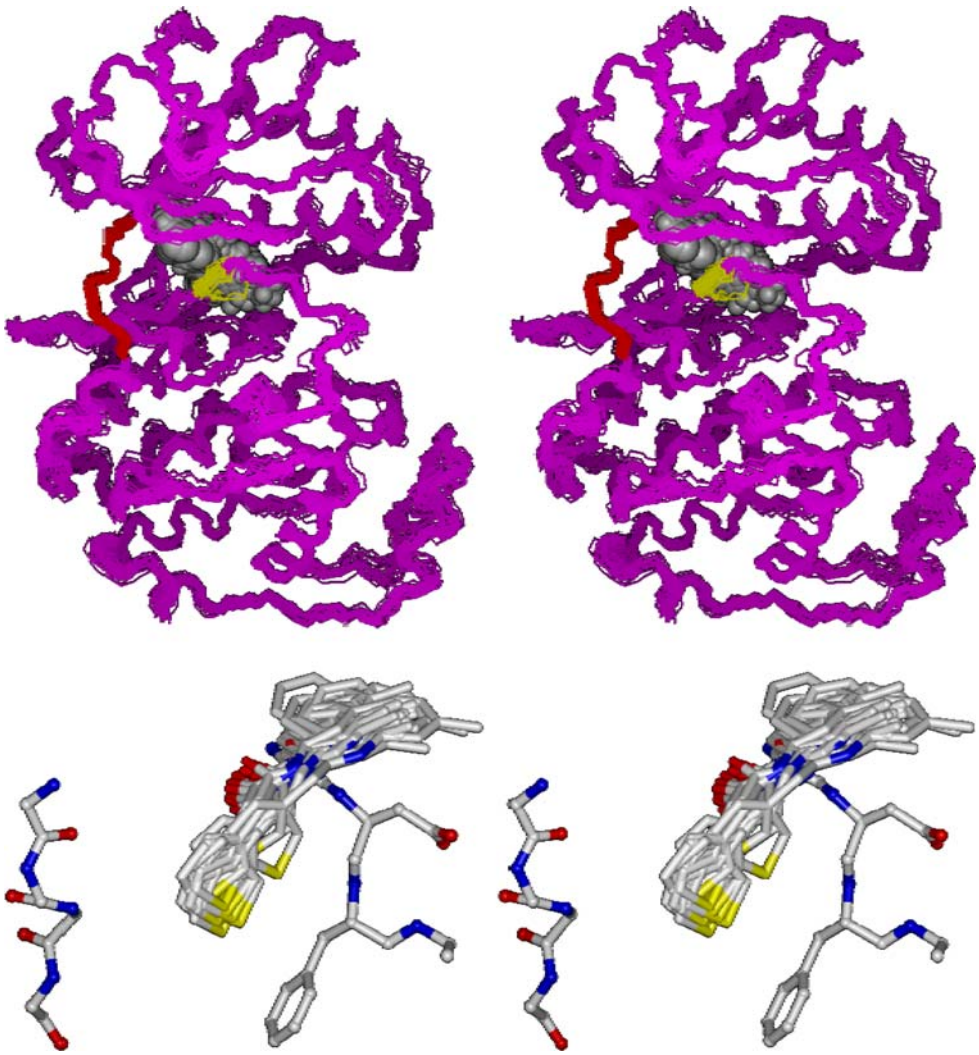

Fig. 9 *Top*: Side-by-side stereo presentation of 25 overlaid snapshots taken in 2 ps steps from the 50 ps production phase of the MD simulation. Only the backbone of the kinase is shown (*magenta*), the DFG tripeptide is highlighted in *yellow*, while the hinge backbone is shown in *red*. The superimposed 25 inhibitor configurations are given as CPK models. *Bottom*: Side-by-side stereo presentation of superimposed snapshots of PRS-001007. From the kinase, only the hinge backbone and the DFG tripeptide are depicted explicitely

aromatic ring positioned in the distal part of the deep-pocket, the fragment drifts out of the binding pocket loosing any hydrogen-bonding interaction with the pharmacophore-establishing moieties of Glu-71 and Asp-168, respectively. For fragment PRS-000058 a comparable tendency emerges as found for the other two fragment hits, in that one binding pose seems to be more favored. Again, only the docking pose in which the di-fluoro-phenyl ring is accommodated by the proximal part of the deep-pocket remains stable over the 50 ps high-energy MD simulations, retaining the hydrogen bond interactions to Asp-168 and Glu-71 (Figure M5, lower panel, left, while the reverse binding mode produces a trajectory, along which the fragment drifts out towards the surface-oriented epitopes of the protein kinase Fig. 10, lower panel, right).

The protein-mediated superposition of distinct snapshots taken in equidistant time steps from the 50 ps MD simulation reveals that the hydrogen bonding potential of e.g., the central amide (PRS-001007—Fig. 10) anchors the fragment in its binding site, while the peripheral thiophene and tolyl rings explore more extended spatial areas, thus providing chemistry various options to improve sterical fit and to evolve the fragment towards the adenine binding region in the appropriate vectorial orientation.

In summary, the devised modelling strategy delivers a consistent picture of the most plausible binding modes of some of the identified fragments. However, we do emphasize that the procedure is based on a variety of assumptions and very much reductionistic in nature. Consequently, we see those results as a framework model in which the experimental results can be explained in a consistent manner, but we are perfectly aware that those model will have flaws and weaknesses which prevent us from reading those models with a spatial resolution at an atomic level.

Conclusion

In summary, the small fragments PRS-000419, PRS-000223 PRS-000058 and the small published BIRB 796

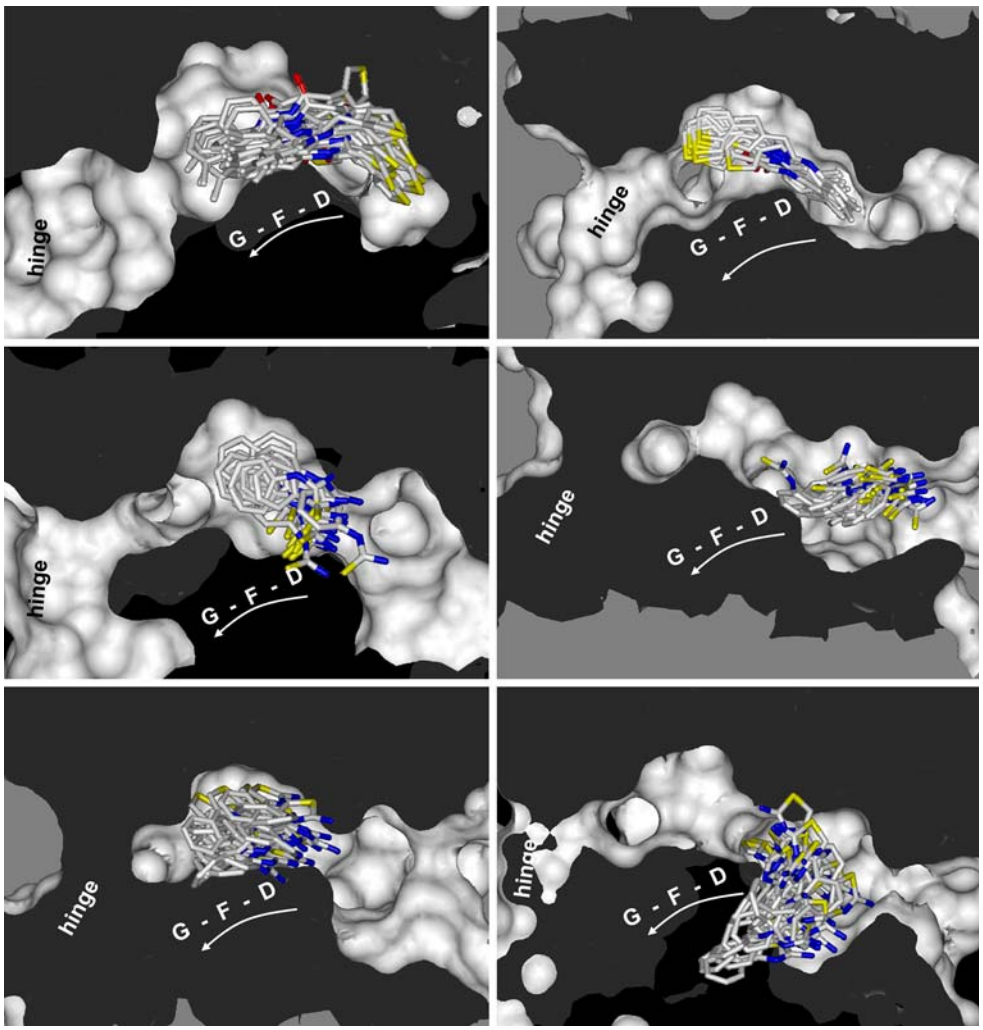

Fig. 10 Superposition of 25 snapshots taken in equidistant steps of 2 ps from the 50 ps MD trajectory for binding mode 1 (*left*) and binding mode 2 (*right*) for all three fragment hits. For the superposition of those snapshots, the C-alpha atoms of the protein kinase have been used. For reasons of clarity, parts of the DFG loop have been removed. Inhibitor molecules are shown in a *stick model* (heavy atoms only), while the binding site is represented by a Connolly surface generated for the averaged protein conformation over the MD simulation

fragment containing the *N*-methyl-pyrazole show low affinities and fast binding kinetics. However, a hypothetical fragment evolution leading to the larger BIRB 796 fragment (*N*-tolyl-pyrazole) and finally to BIRB 796 demonstrates the viability of a stepwise design of compounds with a prolonged residence time and a high affinity. However, it should be emphasized that the underlying strategy and the fragments that have been chosen for in-depth analysis resemble a retrospective approach in which the final inhibitor, i.e., BIRB 796 was known at the outset of the study and served as blueprint for compound selection. A corresponding prospective approach would require a detailed binding and activity determination, combined with molecular docking of numerous fragments in order to guide a fragment linking or fragment evolution strategy in the absence of a final inhibitor. Based on biochemical and in silico structural analysis a medicinal chemistry approach could be devised trying to minimize the otherwise combinatorial nature of fragment merging. For such an approach, fragments which potentially address distinct, but partially overlapping regions of the illuminated binding pocket would be proposed to be linked. We are convinced that iterative optimization including repetitive biochemical characterization, in silico docking, and chemical synthesis will inform the lead finding campaign and more stringently yield high-affinity compounds with the desired engineered binding kinetic attributes when compared to traditional approaches such as combinatorial extensions of once identified seed fragments.

Acknowledgments We are grateful to Stephanie Gspurning and Birgit Flicke for excellent technical assistance.

References

1. Congreve M, Chessari G, Tisi D, Woodhead AJ (2008) J Med Chem 51:3661–3680. doi:10.1021/jm8000373
2. Hann MM, Leach AR, Harper G (2001) J Chem Inf Comput Sci 41:856–864. doi:10.1021/ci000403i
3. Hann MM, Oprea TI (2004) Curr Opin Chem Biol 8:255–263. doi:10.1016/j.cbpa.2004.04.003
4. Sutherland JJ, Higgs RE, Watson I, Vieth M (2008) J Med Chem 51:2689–2700. doi:10.1021/jm701399f
5. Babaoglu K, Shoichet B (2006) Nat Chem Biol 2:720–723. doi:10.1038/nchembio831
6. Copeland RA, Pompliano DL, Meek TD (2007) Nat Rev Drug Discov 5:730–739. doi:10.1038/nrd2082
7. Swinney DC (2004) Nat Rev Drug Discov 3:801–808. doi:10.1038/nrd1500
8. Swinney DC (2006) Curr Top Med Chem 6:461–478. doi:10.2174/156802606776743093
9. Wood ER, Truesdale AT, McDonald OB (2004) Cancer Res 64:6652–6659. doi:10.1158/0008-5472.CAN-04-1168
10. Backes AC, Zech B, Felber B, Klebl B, Müller G (2008) Expert Opin Drug Discov 3:1409–1425. doi:10.1517/17460440802579975
11. Backes AC, Zech B, Felber B, Klebl B, Müller G (2008) Expert Opin Drug Discov 3:1427–1449. doi:10.1517/17460440802580106
12. Pargellis C, Tong L, Churchill L, Cirillo PF, Gilmore T, Graham AG (2002) Nat Struct Biol 9:268–272. doi:10.1038/nsb770
13. Regan J, Pargellis CA, Cirillo PF, Gilmore T, Hickey ER, Peet GW (2003) Bioorg Med Chem Lett 13:3101–3104. doi:10.1016/S0960-894X(03)00656-5
14. Frembgen-Kesner T, Elcock AH (2006) J Mol Biol 359:202–214. doi:10.1016/j.jmb.2006.03.021
15. Gill AL, Frederickson M, Cleasby A, Woodhead SJ, Carr MG, Woodhead AJ, Walker MT, Congreve MS, Devine LA, Tisi D, O'Reilly M, Seavers LC, Davis DJ, Curry J, Anthony R, Padova A, Murray CW, Carr RA, Jhoti H (2005) J Med Chem 48:414–426. doi:10.1021/jm049575n
16. Dauber-Osguthorpe P, Roberts VA, Osguthorpe DJ, Wolff J, Genest M, Hagler MT (1988) Protein Struct Funct Genet 4:31. doi:10.1002/prot.340040106
17. Cheng Y-C, Prusoff WH (1973) Biochem Pharmacol 22:3099–3108. doi:10.1016/0006-2952(73)90196-2
18. Zaman GJ, van der Lee MM, Kok JJ, Nelissen RL, Loomans EE (2006) Assay Drug Dev Technol 4(4):411–420